

Conditional Diffusion Feature Refinement for Continuous Sign Language Recognition

Leming Guo*

School of Computer Science and Engineering, Tianjin University of Technology, Tianjin China
glm@stud.tjut.edu.cn

Wanli Xue[†]

School of Computer Science and Engineering, Tianjin University of Technology, Tianjin China
xuewanli@email.tjut.edu.cn

Qing Guo

Centre for Frontier AI Research (CFAR), A*STAR, Singapore China
tsingqguo@ieee.org

Yuxi Zhou

School of Computer Science and Engineering, Tianjin University of Technology, Tianjin China
joy_yuxi@pku.edu.cn

Tiantian Yuan

Technical College for the Deaf, Tianjin University of Technology, Tianjin China
yuantt@tjut.edu.cn

Shengyong Chen

School of Computer Science and Engineering, Tianjin University of Technology, Tianjin China
sy@ieee.org

ABSTRACT

In this work, we are dedicated to leveraging the denoising diffusion models' success and formulating feature refinement as the autoencoder-formed diffusion process, which is a mask-and-predict scheme. The state-of-the-art CSLR framework consists of a spatial module, a visual module, a sequence module, and a sequence learning function. However, this framework has faced sequence module overfitting caused by the objective function and small-scale available benchmarks, which results in model insufficient training. To overcome the overfitting problem, some CSLR studies enforce the sequence module to learn more visual temporal information or be guided by more informative supervision to refine its representations. In this work, we first conduct a conditional diffusion feature refinement (CDR) to directly produce the sequence representations with desired properties *i.e.*, the effective short-long-term temporal dependencies, and be more discriminate. However, due to the small-scale data, the generated sequence representations by CDR are semantic corruption. Therefore, to overcome this problem, we propose a novel autoencoder-formed conditional diffusion feature refinement (ACDR) to refine the sequence representations to equip desired properties by learning the encoding-decoding optimization process in an end-to-end way. Specifically, for the ACDR, a noising Encoder is proposed to progressively add noise equipped with semantic conditions to the sequence representations. And a denoising Decoder is proposed to progressively denoise the noisy sequence representations with semantic conditions. Therefore, the sequence representations can be imbued with the semantics of provided semantic conditions. Further, a semantic constraint is employed to prevent the denoised sequence representations from semantic corruption. Notice that the ACDR can be viewed as an additional component applied to other methods with a similar framework. Extensive experiments are conducted to validate the effectiveness of our ACDR, benefiting state-of-the-art methods and achieving a notable gain on three benchmarks.

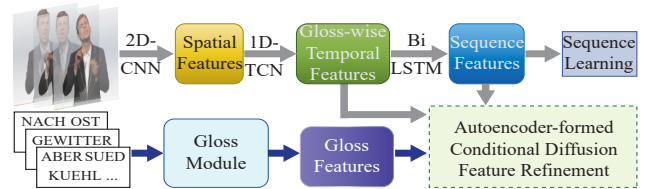


Figure 1: Overview of the proposed ACDR approach. The ACDR conducts an encoding-decoding optimization form to add noise and denoise with semantic conditions to implicitly refine the sequence representations modeling effective short-long-term temporal dependencies and be more discriminate.

1 INTRODUCTION

Sign language is a visual language that hearing-impaired people mainly rely on hand shape, hand position, hand orientation, human movement, and facial expression to understand sign language [32]. Further, continuous sign language recognition (CSLR) involves capturing these elements of videos to recognize them to their corresponding sign language glosses. Therefore, CSLR can improve the efficiency of understanding the intention of hearing-impaired people, and CSLR has received increasing attention from researchers [1, 27].

The current state-of-the-art framework for CSLR involves a spatial module to extract frame-wise spatial information, a visual module to capture gloss-wise temporal information, and a sequence module to model short-long-term temporal context and the sequence information, *i.e.*, signs order. Finally, the baseline is optimized by the Connectionist Temporal Classification (CTC) [9] loss function. This baseline has witnessed the limitation where the sequence module is prone to overfitting, which makes its representations difficult to provide effective short-long-term temporal information for recognition and also leads to insufficient optimization information provided in backpropagation. Further, this limitation is aggravated by small-scale datasets, resulting in a challenge to strengthening the sequence representations' generalization ability.

Currently, some methods [7, 11, 23–25, 39] proposed temporal consistency schemes to enforce the sequence module to concentrate more on the gloss-wise temporal information learning to alleviate its overfitting. In addition, some works dedicate to guiding the CSLR model’s representations to be more discriminated to enhance the generalization ability of the sequence representations, such as [24, 25] and [39] employed gloss and pose keypoints location as extra supervision, and [16, 17, 21] enforce to capture body trajectories to identify signs. According to the above state-of-the-art works, we notice that the desired sequence representation should have these desired properties, *i.e.*, effective short-long-term temporal dependencies, and be more discriminative. *Such desired properties make access to the suitable sequence representation challenging.*

Inspired by the success of the conditional diffusion model [10, 22, 28–30], which has powerfully capable of generating the desired output equipped with the given condition (*i.e.*, the text sentence), an intuitive idea is to utilize the diffusion process fed into extra conditions to generate the desired sequence representation. In this work, we first conduct a conditional diffusion feature refinement in Sec. 3.2 to achieve the goal via the mask-and-predict scheme. However, limited by the small-scale training data, this refinement is unavailable to generate the desired sequence representations, even resulting in semantic corruption.

To overcome this problem, we propose an autoencoder-formed conditional diffusion feature refinement (ACDR) that the conditional diffusion feature refinement is also adopted, and an advanced optimization is further proposed. Firstly, the ACDR conducts a noising Encoder to progressively add noise equipped with semantic conditions to the sequence representations, and then the 1D-UNet will be optimized to predict the noisy sequence representations to the random Gaussian noise. Secondly, a denoising Decoder is proposed to progressively denoise the the noisy sequence representations with the semantic conditions, which is able to be imbued with the semantics of provided semantic conditions. Further, a semantic constraint is employed to prevent the denoised sequence representations from semantic corruption. Consequently, through the optimization of ACDR, the sequence representations can be refined to achieve these properties by focusing on learning the encoding-decoding process in an end-to-end way rather than directly learning the target representations. Notice that the ACDR can be viewed as an additional component applied to all methods based on the baseline and suffering from the easy-overfitting problem. Moreover, we also use a recent interpretation method (*i.e.*, the compression of information stored in weights (IIW) [34]) to evaluate the generalization capability of the ACDR-optimized sequence representations (See the supplementary material).

2 RELATED WORK

2.1 Continuous sign language recognition

The CSLR forces on the scenario where a video corresponds to a sequence of glosses, and the order of each gloss is consistent with signs in the video. Due to only sentence-level annotations and small-scale data being available in current CSLR datasets, how to utilize the data to learn stronger video representations to accurately recognize glosses, remains a fundamental research problem. In the

past, under the weakly annotated data, many state-of-the-art approaches exploit the connectionist temporal classification (CTC)[9] to provide frames-wise supervision by maximizing the probabilities of all alignments paths between frames and glosses that are able to achieve by a mini-batch optimized. On the other hand, many state-of-the-art methods [8, 11, 16, 17, 21, 23, 36] consider that the baseline involves a spatial module, a visual module, a sequential module, and the CTC constraint can achieve effective performance. However, this baseline has faced an insufficient optimizing problem caused by the easy-overfitting sequence module, whose pool generalization representations are unable to offer sufficient temporal information to recognize signs effectively.

To mitigate this overfitting problem, some recent methods [11, 23, 39] conduct temporal alignment constraints, which aim to directly refine the sequence representations to model more effective short-long-term dependencies by enforcing the sequence module focusing on learning gloss-wise temporal information. In addition, some approaches [5, 7, 11, 16, 17, 21, 36] introduce additional supervision information to enhance the CSLR model to implicitly make the sequence representations be more discriminate. For instance, [7] and [11] produce an end-to-end epoch-wise fine-tuning strategy to produce frames-wise labels to boost the CSLR model. [21] focuses on squeezing temporal features that can capture multi-temporal patterns glosses and [16, 17, 39] aims to exploit pose heatmaps or body trajectories to dynamically emphasize informative sign spatial regions. [5, 36] exploits the pre-trained model to provide extensive external supervision to achieve cross-modal alignment, which also improves the discrimination of the sequence representations. Different from these methods, our method is driven to employ the powerful conditional diffusion model to implicitly refine the sequence representations to model more effective short-long-term dependencies and be more discriminate.

2.2 Denoising diffusion models

The denoising diffusion model incorporates a forward Gaussian diffusion noising process and a reverse denoising generation process, which is able to refine the generated objects starting from Gaussian noise iteratively. The denoising diffusion model has been shown to be impressive and powerful for text-to-video generation and text-to-video generation such as Imagen [30], DALLE-2 [26], Stable Diffusion [28], Video diffusion model [15], Imagen Video [14] and MM-Diffusion [29]. In addition, denoising diffusion models have also shown significant potential in the fields of image caption [38], [13], image classification [10], and image segmentation [20], [35], [2]. [22] and [13] add noise to the text with the image conditions to learn the forward diffusion process, and then generate the corresponding caption according to the image conditions in the reverse diffusion process. [10], [20], [35], [2] also regard the image as the condition and add noise to the ground-truth to learn the forward diffusion process, and finally generate the corresponding ground-truth via the denoising diffusion process. In this work, we employ the denoising diffusion model strategy to refine the sequence representations equipped with semantic conditions to model practical short-long-term temporal dependencies and be more discriminative.

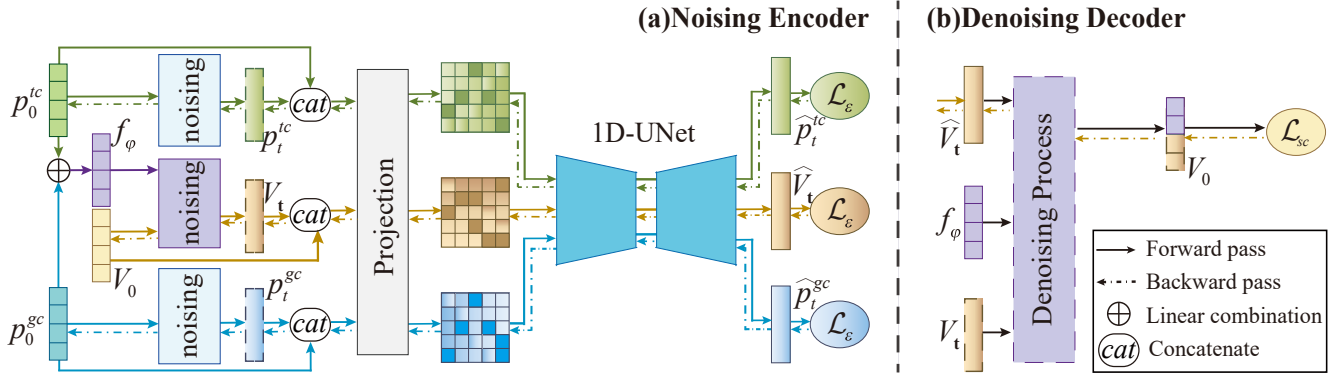


Figure 2: Pipeline of the proposed ACDR. The SCPM focuses on improving feature diversity. The ACDR is an autoencoder-formed framework containing a noising Encoder and a denoising Decoder. The Encoder works on adding noise with semantic conditions to sequence representation and learns added noise. The Decoder aims to denoising the noised representation with semantic conditions to achieve semantic refinement and reserve the original semantic.

3 PRELIMINARIES AND ANALYSIS

3.1 General Baseline of CSLR

One sign language video is always made up of contiguous signs and their corresponding glosses, which are two sequences following the sign language syntactic structure [32]. Current state-of-the-art CSLR works [11, 16, 17, 21, 23, 36, 39] have noticed that the high-performance baseline framework ϕ always follows a cascaded architecture, it comprises a spatial module ϕ_{spm} , a visual module ϕ_{vm} , a sequence module ϕ_{sem} and a sequence learning function \mathcal{H} .

Formally, given one sign language video sequence with T frames $\mathcal{X} = \{x^i\}_{i=1}^T$, and its ground-truth sentence with L glosses $\mathcal{Y} = \{y^i\}_{i=1}^L$, which is annotated at sentence-level, the CSLR task dedicates to learn an alignment $\mathcal{Y} = \phi(\mathcal{X})$. Specifically, the 2DCNN *i.e.*, ResNet18 [12] is leveraged to be ϕ_{spm} , ϕ_{vm} , ϕ_{sem} are empirically set to variants or normal temporal convolution networks (1D-TCNs) [5, 11, 16, 17, 21, 23, 39] and Bi-Lstm [11, 16, 17, 21, 23, 36, 39], and \mathcal{H} is set to the connectionist temporal classification (CTC) loss [5, 6, 11, 16, 17, 21, 23, 36, 39].

In practice, ϕ_{spm} first extracts spatial features $X_{sp} = \{x_{sp}^i\}_{i=1}^T$ from \mathcal{X} . Then, ϕ_{vm} will model gloss-wise temporal features $X_{gwt} = \{x_{gwt}^i\}_{i=1}^T$ from X_{sp} by establishing adjacent frames correlations and learn sign-specific knowledge. Besides, ϕ_{sem} will excellently model sequential and contextual correlation across X_{gwt} to learn sequence representation $V = \{v^i\}_{i=1}^T$. Moreover, V are fed into the classifier ϕ_{F_v} to predict corresponding logits $Z_V = \{z_V^i\}_{i=1}^T$. Finally, \mathcal{H} enables to alignments between Z_V and \mathcal{Y} , and computes losses. Specifically, during test stage, the predicted ground-truth sequence $\mathcal{Y}_p = \{y_p^i\}_{i=1}^L$ will be derived from Z_V via the learned \mathcal{H} straightly.

3.2 Conditional Diffusion Feature Refinement

Due to the small-scale data and the CTC optimization, the easy-overfitting problem of the sequence module in the state-of-the-art baselines occurs, which affects the final prediction performance. To overcome this problem, some methods [7, 11, 23–25, 39] introduce extra supervision to enforce the sequence module learn more to produce representations with effective short-long-term temporal

dependencies and be more discriminative. Inspired by the success of the diffusion model [10, 13–15, 20, 26, 28–30], we explore imposing an end-to-end feature refinement method, *i.e.*, condition diffusion feature refinement (CDR), which utilizes the diffusion process fed into extra conditions to generate the desired sequence representations. And we first conduct preliminaries to study the feature refinement method. The condition diffusion feature refinement comprises a diffusion module (1D-UNet), the noising refinement process, and the denoising refinement process. And to achieve the desired properties, the condition diffusion feature refinement extracts the gloss-wise temporal information and gloss information as semantic conditions for the semantic complementarity in terms of both local temporal context and categorical correlation.

Gloss-wise temporal condition. Specifically, we extract the channel knowledge from the gloss-wise temporal features X_{gwt} via the softmax operation to conduct the gloss-wise temporal condition p^{tc} :

$$p^{tc} = \frac{e^{(x_{gwt}^i)}}{\sum_{j=1}^T e^{(x_{gwt}^j)}} \quad (1)$$

Gloss condition. Because the gloss feature representation can be regarded as the discriminative and important feature that spans many dimensions in visual feature space, we quantify the sequence representation V to produce the gloss condition p^{gc} , inspired by the VQ-VAE [33]. Specifically, we first conduct a codebook via a pre-trained gloss embedding [6] to provide discrete latent variables e , which follow categorical distributions. Then the quantified representation p^{gc} will be computed by the nearest neighbor look-up between sequence representations V and discrete latent variables e in the codebook.

$$(p^{gc})^i = e^k, k = \operatorname{argmin}_j \|v^i - e^j\|_2, \quad (2)$$

where the look-up operation is the representation V mapped onto the nearest element of gloss embedding e .

The diffusion noising process. For this process, the CSLR baseline in Sec. 3.1 is adopted as the backbone to extract the sequence representation V . And then, the Gaussian noise ε is incrementally added to the sequence representation V_0 ($V_0 = V$) conditioned

on the diffusion step t and semantic conditions f_ϕ , which can be represented as the Markov chain $q(V_t|V_{t-1}, f_\phi)$. As a result, all intermediate noisy latent variables are denoted as $V_{1:t}$, and V_t is the noisy sequence representation with Gaussian distribution. Specifically, the diffusion step t is sampled from a uniform distribution of $[1, t]$. And the diffusion schedule for Gaussian noise added to the sequence representation v at diffusion step t is pre-defined as a linear noise schedule $\{\beta_t\}_{n=1:t} \in (0, 1)^t$. Consequently, inspired by the CARD [10], given the semantic condition f_ϕ , the noising process conditional distributions are specified in the same fashion as the CARD [10]:

$$q(V_t|V_0, f_\phi) = \mathcal{N}(V_t; \sqrt{\alpha_t}V_0 + (1 - \sqrt{\alpha_t})f_\phi, (1 - \alpha_t)\mathbf{I}), \quad (3)$$

where all diffusion steps including $t = 1$, $\alpha_t := 1 - \beta_t$, and $\bar{\alpha}_t := \prod_t \alpha_t$, the semantic condition f_ϕ can be set to a linear combination ($\tau \times p^{tc} + (1 - \tau) \times p^{gc}$). Furthermore, given the sequence representation V and the semantic conditions p^{tc} and p^{gc} , and the 1D-UNet ε_ϕ , the diffusion noising process can be optimized by the condition reconstruction regularization \mathcal{L}_ε :

$$\mathcal{L}_\varepsilon = \left\| \varepsilon - \varepsilon_\phi \left(x, \sqrt{\alpha_t}V_0 + \sqrt{1 - \alpha_t}\varepsilon + (1 - \sqrt{\alpha_t})f_\phi, f_\phi, t \right) \right\|^2, \quad (4)$$

where in the 1D-UNet, all convolution layers have 1D kernel size, and the 1D-UNet is optimized to learn the added noise at each denoise step t via the condition reconstruction regularization.

The diffusion denoising process. In this part, we also follow the denoising form of [10] to achieve the denoising process. For Equation 3, such formulation corresponds to a tractable noising process posterior:

$$q(V_{t-1}|V_t, V_0, f_\phi) = \mathcal{N}(V_{t-1}; \mu(V_t, V_0, f_\phi), \tilde{\beta}_t \mathbf{I}), \quad (5)$$

where

$$\mu := \lambda_0 V_0 + \lambda_1 V_t + \lambda_2 f_\phi(x), \quad (6)$$

and where $\tilde{\beta}_t := \frac{1 - \bar{\alpha}_{t-1}}{1 - \bar{\alpha}_t} \beta_t$, $\lambda_0 = \frac{\beta_t \sqrt{\bar{\alpha}_{t-1}}}{1 - \bar{\alpha}_t}$, $\lambda_1 = \frac{(1 - \bar{\alpha}_{t-1}) \sqrt{\bar{\alpha}_t}}{1 - \bar{\alpha}_t}$, and $\lambda_2 = 1 + \frac{(\sqrt{\bar{\alpha}_t} - 1)(\sqrt{\bar{\alpha}_t} + \sqrt{\bar{\alpha}_{t-1}})}{1 - \bar{\alpha}_t}$.

Based on the noising process posterior (Equation 5), the predicted noise representations \widehat{V}_t produced by the 1D-UNet ε_θ will be denoised with semantic conditions f_ϕ by a Markov chain process over variables $\widehat{V}_t \dots \widehat{V}_0$ to generate the desired sequence representations \widehat{V}_0 owning the semantic supervision of both gloss-wise temporal features and gloss features. The diffusion denoising process can be formulated as follows:

$$\widehat{V}_0 = \frac{1}{\sqrt{\bar{\alpha}_t}} \left(\widehat{V}_t - (1 - \sqrt{\bar{\alpha}_t}) f_\phi(x) - \sqrt{1 - \bar{\alpha}_t} \varepsilon_\theta(x, \widehat{V}_t, f_\phi(x), t) \right), \quad (7)$$

$$\widehat{V}_{t-1} = \lambda_0 \widehat{V}_0 + \lambda_1 \widehat{V}_t + \lambda_2 f_\phi(x) + \sqrt{\beta_t} \varepsilon, \text{ if } t > 1, \quad (8)$$

where if $t \leq 1$, $\widehat{V}_{t-1} = \widehat{V}_0$. Intuitively, through the denoising process, the denoised sequence representations \widehat{V}_0 are able to be imbued with the semantics of provided semantic conditions. And \widehat{V}_0 will be fed into the classifier Z_V to generate the final prediction and then optimized by the CTC loss.

3.3 Problems and Motivations

Problem of the current diffusion feature refinement. In the above preliminaries, we aim to develop the desired sequence representations \widehat{V}_0 , which should contribute more to effective short-long-term temporal dependencies, and be more discriminative, thus performing more effectively. However, as shown in Table 1, we observe that the denoised sequence representations \widehat{V}_0 is unable to achieve an improvement, even obtains quite worse performance, and the CTC loss is difficult to achieve good convergence. As a result, we explore evaluating the quality of \widehat{V}_0 by adopting the maximum-mean discrepancy (MMD) and the KL-divergence to measure the difference from the initial sequence representations V_0 . And we observe that both the MMD value and the KL loss are very large. These experiments phenomena demonstrate that limited by the small-scale training data, the denoised sequence representations \widehat{V}_0 can not have the desired optimization via the conditional diffusion feature refinement. The original semantics of the sequence module in the denoised sequence representations \widehat{V}_0 may be broken, leading to bad results. Our aim is to achieve semantic complementation for the feature refinement rather than semantic corruption, which defeats our original intent.

Table 1: Ablation study on the CDR and compatibility to other stat-of-the-art CSLR methods on the RWTH-2014 dataset. C_{tc} and C_{gc} indicate employing the gloss-wise temporal condition and gloss condition in the CDR optimization.

Methods	C_{tc}	C_{gc}	Dev (%) ↓	Test (%) ↓
VAC [23]			21.2	22.3
+CDR	✓	✓	94.5	94.8
VAC+SMKD [11, 23]			19.8	20.8
+CDR	✓	✓	93.2	93.9
TLP [21]			19.7	20.8
+CDR	✓	✓	93.3	93.6
SEN [17]			19.5	21.0
+CDR	✓	✓	93.1	94.7
CorrNet [16]			19.0	19.7
+CDR	✓	✓	92.5	93.4

Motivations. According to the above preliminaries, limited by the small-scale training data, it is unavailable for the conditional diffusion feature refinement to generate the desired sequence representations. Because the sequence representations are directly related to the final accuracy, the key problem becomes *how to design an advanced optimization strategy to refine the sequence representations*. Consequently, all the above preliminaries motivate us to develop an advanced conditional diffusion feature refinement, which enforces the sequence representations to emphasize effective short-long-term temporal dependencies, being more discriminative and reserving the original semantic distribution.

4 AUTOENCODER-FORMED CONDITIONAL DIFFUSION FEATURE REFINEMENT

In this section, inspired by the MAE that achieves feature refinement by learning the denoising process, we propose an autoencoder-formed conditional diffusion feature refinement (ACDR) to implicitly refine the sequence representations by focusing on learning the encoding-decoding process. Figure 2 shows the illustration of the ACDR framework. Specifically, the ACDR conducts a noising Encoder for noise learning, which involves the diffusion noising process in Sec. 3.2 and conducts a denoising Decoder for denoised representation constraint, which includes the diffusion denoising process in Sec. 3.2.

Noising Encoder. Given the sequence representation V ($V = V_0$), the 1D-UNet ε_θ , and the semantic conditions $f_\phi = (\tau \times p^{tc} + (1 - \tau) \times p^{gc})$, the noising Encoder will first obtain the noisy sequence representations V_t via the Equation 3 of the diffusion noising process in Sec. 3.2. Further, to emphasize the gloss-wise temporal condition p^{tc} ($p^{tc} = p_0^{tc}$) and the gloss condition p^{gc} ($p^{gc} = p_0^{gc}$), we also apply the diffusion noising process on them to generate corresponding noisy variables p_t^{tc} and p_t^{gc} . Then, V_t , p_t^{tc} and p_t^{gc} are concatenated with their corresponding non-noisy variables V_0 , p_0^{tc} and p_0^{gc} on the channel dimension and project them into a latent space respectively to recover the dimension. Finally, three projected representations are fed into the 1D-UNet and produce the predicted noise representations \widehat{V}_t , \widehat{p}_t^{tc} and \widehat{p}_t^{gc} . \widehat{V}_t , \widehat{p}_t^{tc} and \widehat{p}_t^{gc} will be optimized by the condition reconstruction regularization \mathcal{L}_ε (Equation 4) to learn noises at each diffusion step t . Specifically, because \widehat{p}_t^{tc} and \widehat{p}_t^{gc} have no condition when acting on them, the ε_θ part in \mathcal{L}_ε (Equation 4) will be replaced with themselves.

Denoising Decoder. Based on the diffusion denoising process in Sec. 3.2 and the noising Encoder process, the denoising Decoder also meets the tractable noising process posterior (see Equation 5). Therefore, given the noisy sequence representations V_t , the semantic conditions $f_\phi = (\tau \times p^{tc} + (1 - \tau) \times p^{gc})$, the denoising Decoder first denoises the predicted noise representations \widehat{V}_t with diffusion step t to generate the denoised representations \widehat{V}_0 via the Equation 7 and the Equation 8. Through this denoising, the denoised sequence representations \widehat{V}_0 are able to be imbued with the semantics of provided semantic conditions. It is also notable that because the noising process (Equation 7) in the noising Encoder follows the Markov chain, as a result, Equation 7 and Equation 7 can naturally adopt the DDIM sampler [31] for fast denoising process. Furthermore, the denoising Decoder is additionally optimized by the semantic constraint \mathcal{L}_{sc} to reserve the semantic of the original sequence representation V .

$$\mathcal{L}_{sc} = D_\phi \left(\widehat{V}_0, V \right), \quad (9)$$

where D_ϕ is set to the feature distribution measurement, such as the joint multiple kernel maximum-mean discrepancy (JMMD), the maximum-mean discrepancy (MMD), or the mean squared loss (MSE). And \mathcal{L}_{sc} dedicated to preventing the distribution of the denoised sequence representation \widehat{V}_0 from having semantic corruption. In this way, the ACDR is able to implicitly refine the sequence

representations V end-to-end by allowing V to learn the encoding-decoding optimization process, rather than explicitly learning the complicated target features.

Objective. Consequently, the objective of the ACDR can be formulated as follows:

$$\mathcal{L}_{ACDR} = \gamma_1 \mathcal{L}_\varepsilon + \gamma_2 \mathcal{L}_{sc}, \quad (10)$$

where the γ_1 and γ_2 are hyperparameters for balance the contribution of the \mathcal{L}_{ACDR} . Further, while optimizing the sequence representation, the ACDR can also optimize the gloss-wise temporal and spatial representation by back-propagation schemes, enhancing their power. It is worth noticing that the ACDR can be viewed as an additional component that can be applied to all methods based on the baseline and suffering from the easy-overfitting problem, being able to enhance their sequence representation and alleviate the overfitting problem.

Table 2: Compatibility to other stat-of-the-art CSLR methods on the RWTH-2014 dataset. Adding ACDR leads to a consistent performance boost. The best results and ACDR results are marked as bold and underlined, respectively.

Methods	Dev (%) ↓		Test (%) ↓	
	del/ins	WER	del/ins	WER
CMA[24]	7.3/2.7	21.3	7.3/2.4	21.9
SMKD[11]	6.8/2.5	20.8	6.3/2.3	21.0
C^2 SLR[39]	-	20.5	-	20.4
CVT-SLR [36]	6.4/2.6	19.8	6.1/2.3	20.1
TwoStream-SLR[6]	-	18.4	-	18.8
VAC[23]	7.9/2.5	21.2	8.4/2.6	22.3
+ACDR	5.5/3.5	<u>20.5</u>	5.8/2.9	<u>20.6</u>
SEN [17]	5.8/2.6	19.5	7.3/4.0	21.0
+ACDR	5.5/2.6	<u>18.8</u>	5.4/2.7	<u>20.0</u>
TLP[21]	6.3/2.8	19.7	6.1/2.9	20.8
+ACDR	5.2/2.9	<u>19.0</u>	5.2/3.1	<u>20.0</u>
CorrNet[16]	5.6/2.8	19.0	5.7/2.3	19.7
+ACDR	4.6/2.9	<u>18.6</u>	5.3/2.6	<u>19.0</u>

5 EXPERIMENTS

5.1 Datasets and Evaluation

RWTH-2014 [19]. It consists of video recordings of weather forecast sign language interpreters delivering 6,842 sentences interpreted by 9 signers, composed of 1,295 sign language vocabulary.

RWTH-2014T[3]. It is a widely utilized resource for continuous sign language recognition (CSLR) and sign language translation (SLT) tasks. It contains 1,085 vocabularies for the CSLR task. All videos are divided into 7,096, 519, and 642 videos for the training, development, and test sets.

CSL-Daily[37]. It is a large Chinese CSLR dataset for both continuous sign language recognition and sign language translation (SLT) tasks. It records 2000 vocabulary and it is divided into 18,401, 1,077,

Table 3: Compatibility to other stat-of-the-art CSLR methods on the RWTH-2014T and CSL-Daily datasets. Adding ACDR leads to a consistent performance boost. The best results and ACDR results are marked as bold and underlined, respectively.

Methods	RWTH-2014T		CSL-Daily	
	Dev (%) ↓	Test (%) ↓	Dev (%) ↓	Test (%) ↓
FCN[7]	23.3	25.1	33.2	32.5
BN-TIN[37]	22.7	23.9	33.6	33.1
SLT[4]	24.6	24.5	33.1	32.0
V-L Mapper[5]	21.9	22.5	-	-
C^2 SLR[39]	20.2	20.4	-	-
TwoStream-SLR[6]	17.7	19.3	25.4	25.3
TLP [21]	19.4	21.2	-	-
+ACDR	<u>17.9</u>	<u>20.4</u>	-	-
SEN [17]	19.3	20.7	31.1	30.7
+ACDR	<u>18.5</u>	<u>20.1</u>	<u>30.0</u>	<u>29.4</u>
CorrNet [16]	18.9	20.5	30.6	30.1
+ACDR	<u>18.3</u>	<u>20.0</u>	<u>29.6</u>	<u>29.0</u>

Table 4: Performance comparison of distinct feature refinement methods on the RWTH-2014 dataset (Upper). And the performance comparison of distinct semantic constraint D_ϕ (Bottom). A_{tc} and A_{gc} indicate employing the gloss-wise temporal condition and gloss condition in the ACDR optimization.

Methods	Knowledge	Dev (%) ↓	Test (%) ↓
VAC	-	21.1	22.3
	A_{tc}	20.8	21.0
	A_{gc}	20.7	20.6
	JMMD	20.7	21.4
	DTW	20.5	20.7
SEN	MMD	19.4	20.2
	MSE	19.6	19.8
	JMMD	19.4	19.8

and 1,176 videos for the training, development, and test sets for the CSLR task.

Evaluation metric. In this work, the word error rate (WER) metric is adopted for the CSLR evaluation. The WER belongs to the edit distance, which measures the minimum number of substitutions (#sub), deletions (#del), and insertions (#ins) operation needed to convert the predicted sentence to the associated reference sentence. The WER calculation method is as follows:

$$WER = \frac{\#sub + \#del + \#ins}{L}, \quad (11)$$

where #sub, #del, #ins are the number of substitutions, deletions, and insertions operation, respectively.

5.2 Implementation Details

Evaluators. In this work, to evaluate the proposed autoencoder-formed conditional diffusion feature refinement (ACDR) by adding it to the current state-of-the-art methods as a component. Specifically, these evaluators have the same baseline framework as the baseline in Sec. 3.1 and encounter the overfitting problem, such as VAC [23], TLP [21], SEN [17], and CorrNet [16]. For both the training and test stages, we follow the data augmentation of the above evaluators.

Autoencoder-formed conditional diffusion feature refinement. In the ACDR, the channels of 1D-UNet are set to 1024. The gloss embedding for the gloss condition in Sec. 3.2 is an embedding layer of one pre-trained model adopted in [5] that has fine-tuned on the CSLR benchmarks [3, 19, 37]. The diffusion step for noising process in the noising Encoder in Sec. 4 is set to 100. And for the denoising Decoder in Sec. 4, D_ϕ is set to the joint multiple kernel maximum-mean discrepancy (JMMD), the DDIM sampler is used for fast sampling, and the diffusion step for the denoising process can be set to 20 (Take 20 random t from $t \in 1000$ at intervals of $1000/20$). The τ in $f_\phi = (\tau \times p^{tc} + (1 - \tau) \times p^{gc})$ of equations can be set to 0.4, and we also conduct ablation studies to evaluate the impact of different τ . The γ_1 and γ_2 in Equation 10 are set to 0.5 and 0.1, respectively, and we also conduct ablation studies to evaluate the impact of different γ_1 and γ_2 .

Training. All evaluators are trained for 50 epochs and optimized by Adam optimizer [18] with an initial learning rate of $1e - 4$, a weight decay factor of $1e - 4$, and batch size of 4. And the learning rate decays (0.2) at 25 and 40 epochs. All experiments are implemented in PyTorch and on one A100 GPU.

5.3 Compatibility to stat-of-the-art methods

Evaluation on RWTH-2014. As shown in Table 2, we can see that with the ACDR optimization, the state-of-the-art methods VAC [23], TLP [21], SEN [17], and CorrNet [16] achieve a remarkably performance improvement (nearly 1%). In particular, the performance of CorrNet is near the multi-modal method TwoStream-SLR [6], which utilizes the pre-captured key points of signs as supervision to help the model learning.

Evaluation on RWTH-2014T. Table 3 also shows that adding ACDR leads to a consistent performance boost on the RWTH-2014T dataset. Especially, the TLP [21] achieves the largest improvement compared to other methods. We consider that the TLP focuses on capturing various temporal pattern signs to preserve discriminative gloss-wise temporal representations, which can provide an effective gloss-wise temporal condition p^{tc} for the ACDR.

Evaluation on CSL-Daily. As shown in Table 3, when adopting the ACDR, both SEN[17] and CorrNet [16] outperform their original method by a large margin (about 1.1%). These experiments validate the effectiveness of the ACDR.

5.4 Ablation Study

In this section, all experiments, except Table 5, are based on the SEN [17] on the RWTH-2014 dataset.

Ablation on ACDR. Table 5 ablates the performance when varying the semantic conditions p^{tc} and p^{gc} . Adding both the gloss-wise temporal condition p^{tc} and the gloss condition p^{gc} can bring better

Table 5: Ablation study on the ACDR and compatibility to other stat-of-the-art CSLR methods on the RWTH-2014 dataset. Adding ACDR leads to a consistent performance boost. A_{tc} and A_{gc} indicate employing the gloss-wise temporal condition and gloss condition in the ACDR optimization.

Methods	A_{tc}	A_{gc}	Dev (%) ↓	Test (%) ↓
Baseline			23.8	25.4
	✓		23.3	24.2
		✓	23.1	24.0
	✓	✓	22.9	23.8
VAC [23]			21.2	22.3
	✓		20.8	21.0
		✓	20.6	20.6
	✓	✓	20.5	20.6
VAC+SMKD [11, 23]			19.8	20.8
	✓		20.1	20.3
		✓	19.8	20.2
	✓	✓	19.6	20.1
TLP [21]			19.7	20.8
	✓		19.3	20.3
		✓	19.2	20.2
	✓	✓	19.0	20.0
SEN [17]			19.5	21.0
	✓		19.7	20.4
		✓	19.1	20.2
	✓	✓	18.8	20.0
CorrNet [16]			19.0	19.7
	✓		18.9	19.2
		✓	18.7	19.1
	✓	✓	18.6	19.0

performance (0.6% and 0.8% on the test set for SEN, 0.5% and 0.6% on the test set for CorrNet, and 0.6% and 1.7% on the test set for VAC). Notably, adopting the gloss condition p^{gc} outperforms the gloss-wise temporal condition p^{tc} by a small gain. This phenomenon is particularly prominent in the results of VAC. We consider that both TLP [21], SEN [17], and CorrNet [16] squeeze more representative temporal features to locate signs with various lengths more precisely, resulting in powerful p^{tc} . However, VAC [23] only aligns the gloss-wise temporal representation to the sequence module representations, which cannot capture signs with various lengths to provide powerful p^{tc} . Furthermore, the pre-trained language embedding layer extracts the gloss condition p^{gc} , which has fine-tuned the CSLR datasets. As a result, the gloss condition p^{gc} can offer rich context information and powerful discriminative information among glosses result in a better performance than p^{tc} . Moreover, adopting both conditions p^{tc} and p^{gc} achieves further performance improvement, which verifies the effectiveness of exploiting the ACDR process to refine the sequence representations. And results

in Table 5 also validate that employing the conditional diffusion process to achieve feature refinement for CSLR is feasible.

Table 6: Ablation study on the γ_1 factor.

γ_1	0.1	0.3	0.5	0.7	1.0
Dev (%) ↓	19.0	19.1	18.8	18.9	19.1
Test (%) ↓	20.2	20.1	20.0	20.1	19.7

Table 7: Ablation study on the γ_2 factor.

γ_2	0.1	0.2	0.4	0.6	0.8
Dev (%) ↓	18.8	19.1	19.1	19.2	19.6
Test (%) ↓	20.0	20.1	20.3	20.4	20.7

Ablation on the distinct γ_1 and γ_2 factors. Table 6 and Table 7 deliver the impact of the noising Encoder and the denoising Decoder from Equation 10. Specifically, for the experiments of Table 6, we set the γ_2 to 0.1, and for the experiments of Table 7, we set the γ_1 to 0.5. We can see that when γ_2 are set to a large value, resulting in worse results, and increasing γ_2 leads to worse performance than γ_1 . However, when the γ_1 is set to 1.0, its performance on the test set achieves improvement. We consider that limited by the small-scale training data, although adopting the semantic constraint \mathcal{L}_{sc} , the model cannot fit the diffusion process well. Therefore, the optimization of the ACDR relies more on the noising Encoder than the denoising Decoder, increasing the contribution of the noising Encoder gains better refinement.

Ablation on the distinct τ factors. In this part, we fix the γ_1 and γ_2 to 0.5 and 0.1, respectively. Figure 3 shows that the recognition performance fluctuates continuously with τ factors increases on the dev set, and the best performance can be achieved when the τ factors reach 0.2-0.5. Notice that $f_\phi = (\tau \times p^{tc} + (1 - \tau) \times p^{gc})$, therefore, τ factor affects the contribution of p^{tc} and p^{gc} . The above results also demonstrate that the achieve a balance contribution for p^{tc} and p^{gc} can achieve better performance.

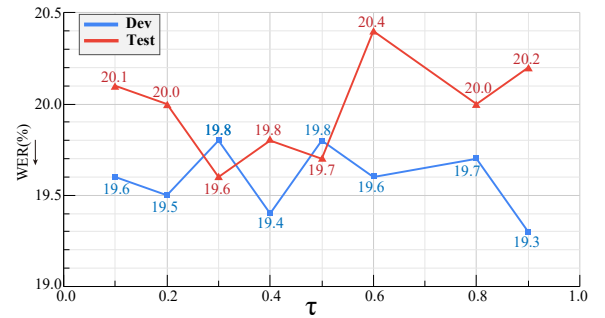


Figure 3: Ablation study on distinct τ factors for the linear combination of semantic conditions.

Ablation on the distinct feature refinement methods and semantic constraints. As shown in Table 4 upper part, we evaluate distinct feature refinement methods on the VAC. We can see that when replacing the knowledge distillation loss with the ACDR gloss-wise temporal condition p^{tc} , the VAC achieves 1.3% WER improvement on the test set. Besides, when comparing the gloss condition p^{gc} with other semantic knowledge transfer methods, the p^{gc} achieves the best performance, which presents the effectiveness of the proposed diffusion refinement. In addition, in Table 4 bottom part, results of distinct semantic constraint \mathcal{L}_{sc} are presented. We observe that the JMMD and MMD outperform the MSE loss, which demonstrates that the denoised sequence representations have equipped with the semantics, strong overly strong constraints can lead to worse results.

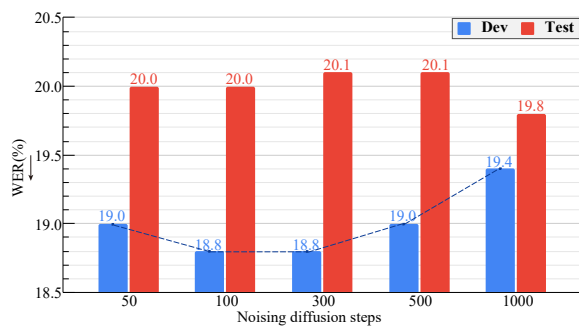


Figure 4: Ablation study on distinct diffusion steps for diffusion noising process.

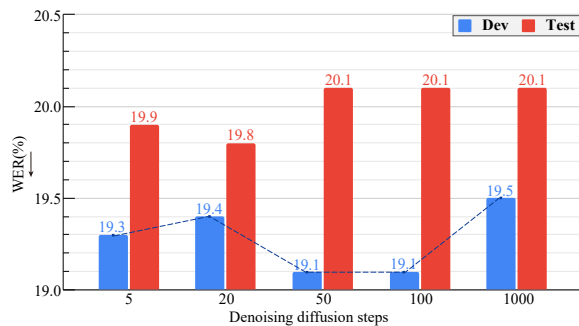


Figure 5: Ablation study on distinct diffusion steps for diffusion denoising process.

Ablation on the diffusion step for both the noising process and denoising process. In this part, we incrementally decrease the diffusion step for the noising process (from 1000 to 50) and the denoising process (from 1000 to 5). Figure 4 ablates that the recognition performance improves as the diffusion step of the diffusion noising process increases, and the best performance is achieved when the diffusion step reaches 300, with the WER of 18.8 on the dev set, after that, the performance gradually decreases. Figure 5 delivers that the recognition performance decreases and then improves as the diffusion step of the diffusion denoising process

increases, and the best performance is achieved when the diffusion step reaches 50 and 100, with the WER of 19.1, after that, the performance gradually decreases.

6 CONCLUSION

In this work, we explore refining the sequence representations via the denoising diffusion model process. We first conduct a conditional diffusion feature refinement (CDR) to directly generate the sequence representations with desired properties *i.e.*, the effective short-long-term temporal dependences, and be more discriminate. However, due to the small-scale training data, the generated sequence representations are semantic corruption. Therefore, to overcome this problem, we propose a novel end-to-end autoencoder-formed conditional diffusion feature refinement (ACDR) to refine the sequence representations to achieve desired properties by learning the encoding-decoding optimization process. Specifically, a noising Encoder is proposed to progressively add noise equipped with semantic conditions to the sequence representations. And a denoising Decoder is proposed to progressively denoise the noisy sequence representations with semantic conditions, which the sequence representations can be imbued with the semantics of semantic conditions. Further, a semantic constraint is employed to preserve the original semantics of the sequence representations. The proposed ACDR can be viewed as an additional component applied to other methods with a similar framework. Experimental results validate the effectiveness of our proposed ACDR, which benefits state-of-the-art methods and achieves a notable gain on three benchmarks.

REFERENCES

- [1] Danielle Bragg, Oscar Koller, Mary Bellard, Larwan Berke, Patrick Boudreault, Annelies Braffort, Naomi Caselli, Matt Huenerfauth, Hernisa Kacorri, Tessa Verhoef, et al. 2019. Sign language recognition, generation, and translation: An interdisciplinary perspective. In *ACM SIGACCESS*.
- [2] Emmanuel Asiedu Brempong, Simon Kornblith, Ting Chen, Niki Parmar, Matthias Minderer, and Mohammad Norouzi. 2022. Denoising Pretraining for Semantic Segmentation. *CVPRW (2022)*, 4174–4185.
- [3] Necati Cihan Camgoz, Simon Hadfield, Oscar Koller, Hermann Ney, and Richard Bowden. 2018. Neural sign language translation. In *CVPR*.
- [4] Necati Cihan Camgoz, Oscar Koller, Simon Hadfield, and Richard Bowden. 2020. Sign language transformers: Joint end-to-end sign language recognition and translation. In *CVPR*.
- [5] Yutong Chen, Fangyun Wei, Xiao Sun, Zhirong Wu, and Stephen Lin. 2022. A Simple Multi-Modality Transfer Learning Baseline for Sign Language Translation. In *CVPR*. 5110–5120. <https://doi.org/10.1109/CVPR52688.2022.00506>
- [6] Yutong Chen, Ronglai Zuo, Fangyun Wei, Yu Wu, Shujie LIU, and Brian Mak. 2022. Two-Stream Network for Sign Language Recognition and Translation. In *NIPS*.
- [7] Ka Leong Cheng, Zhaoyang Yang, Qifeng Chen, and Yu-Wing Tai. 2020. Fully convolutional networks for continuous sign language recognition. In *ECCV*.
- [8] Rungpeng Cui, Hu Liu, and Changshui Zhang. 2019. A deep neural framework for continuous sign language recognition by iterative training. *TMM* 21, 7 (2019), 1880–1891.
- [9] Alex Graves, Santiago Fernández, Faustino Gomez, and Jürgen Schmidhuber. 2006. Connectionist temporal classification: labelling unsegmented sequence data with recurrent neural networks. In *ICML*.
- [10] Xizwen Han, Huangjie Zheng, and Mingyuan Zhou. 2022. CARD: Classification and Regression Diffusion Models. In *NIPS*.
- [11] Aiming Hao, Yuecong Min, and Xilin Chen. 2021. Self-Mutual Distillation Learning for Continuous Sign Language Recognition. In *ICCV*.
- [12] Kaiming He, Xiangyu Zhang, Shaoqing Ren, and Jian Sun. 2016. Deep residual learning for image recognition. In *CVPR*.
- [13] Zhengfu He, Tianxiang Sun, Kuan Wang, Xuanjing Huang, and Xipeng Qiu. 2022. DiffusionBERT: Improving Generative Masked Language Models with Diffusion Models. *ArXiv (2022)*.
- [14] Jonathan Ho, William Chan, Chitwan Saharia, Jay Whang, Ruiqi Gao, Alexey A. Gritsenko, Diederik P. Kingma, Ben Poole, Mohammad Norouzi, David J. Fleet, and Tim Salimans. 2022. Imagen Video: High Definition Video Generation with Diffusion Models. *ArXiv (2022)*.
- [15] Jonathan Ho, Tim Salimans, Alexey Gritsenko, William Chan, Mohammad Norouzi, and David J. Fleet. 2022. Video Diffusion Models. *ArXiv (2022)*.
- [16] Lianyu Hu, Liqing Gao, Zekang Liu, and Wei Feng. 2023. Continuous Sign Language Recognition with Correlation Network. *arXiv preprint arXiv:2303.03202 (2023)*.
- [17] Lianyu Hu, Liqing Gao, Zekang Liu, and Wei Feng. 2023. Self-Emphasizing Network for Continuous Sign Language Recognition. In *AAAI*.
- [18] Diederik P Kingma and Jimmy Ba. 2015. Adam: A Method for Stochastic Optimization. In *ICLR*.
- [19] Oscar Koller, Jens Forster, and Hermann Ney. 2015. Continuous sign language recognition: Towards large vocabulary statistical recognition systems handling multiple signers. *Computer Vision and Image Understanding (2015)*.
- [20] Minh-Quan Le, Tam V. Nguyen, Trung-Nghia Le, Thanh-Toan Do, Minh N. Do, and M. Tran. 2023. MaskDiff: Modeling Mask Distribution with Diffusion Probabilistic Model for Few-Shot Instance Segmentation. *ArXiv abs/2303.05105 (2023)*.
- [21] Zekang Liu Lianyu Hu, Liqing Gao and Wei Feng. 2022. Temporal Lift Pooling for Continuous Sign Language Recognition. In *ECCV*.
- [22] Jian-Hao Luo, Yehao Li, Yingwei Pan, Ting Yao, Jianlin Feng, Hongyang Chao, and Tao Mei. 2022. Semantic-Conditional Diffusion Networks for Image Captioning. *ArXiv (2022)*.
- [23] Yuecong Min, Aiming Hao, Xiujuan Chai, and Xilin Chen. 2021. Visual Alignment Constraint for Continuous Sign Language Recognition. In *ICCV*.
- [24] Junfu Pu, Wengang Zhou, Hezhen Hu, and Houqiang Li. 2020. Boosting continuous sign language recognition via cross modality augmentation. In *ACMMM*.
- [25] Junfu Pu, Wengang Zhou, and Houqiang Li. 2019. Iterative alignment network for continuous sign language recognition. In *CVPR*.
- [26] Aditya Ramesh, Prafulla Dhariwal, Alex Nichol, Casey Chu, and Mark Chen. 2022. Hierarchical Text-Conditional Image Generation with CLIP Latents. *ArXiv abs/2204.06125 (2022)*.
- [27] Razieh Rastgoo, Kourosh Kiani, and Sergio Escalera. 2021. Sign language recognition: A deep survey. *Expert Systems with Applications (2021)*.
- [28] Robin Rombach, A. Blattmann, Dominik Lorenz, Patrick Esser, and Björn Ommer. 2022. High-Resolution Image Synthesis with Latent Diffusion Models. *CVPR (2022)*, 10674–10685.
- [29] Ludan Ruan, Y. Ma, Huan Yang, Huiguo He, Bei Liu, Jianlong Fu, Nicholas Jing Yuan, Qin Jin, and Baining Guo. 2022. MM-Diffusion: Learning Multi-Modal Diffusion Models for Joint Audio and Video Generation. *ArXiv abs/2212.09478 (2022)*.
- [30] Chitwan Saharia, William Chan, Saurabh Saxena, Lala Li, Jay Whang, Emily L. Denton, Seyed Kamyar Seyed Ghasemipour, Burcu Karagol Ayan, Seyedeh Sara Mahdavi, Raphael Gontijo Lopes, Tim Salimans, Jonathan Ho, David J. Fleet, and Mohammad Norouzi. 2022. Photorealistic Text-to-Image Diffusion Models with Deep Language Understanding. *ArXiv (2022)*.
- [31] Jiaming Song, Chenlin Meng, and Stefano Ermon. 2021. Denoising Diffusion Implicit Models. In *ICLR*.
- [32] Rachel Sutton-Spence and Bencie Woll. 1999. *The linguistics of British Sign Language: an introduction*.
- [33] Aaron van den Oord, Oriol Vinyals, and Koray Kavukcuoglu. 2017. Neural Discrete Representation Learning. In *NIPS*. 6309–6318.
- [34] Zifeng Wang, Shao-Lun Huang, Ercan Engin Kuruoglu, Jimeng Sun, Xi Chen, and Yefeng Zheng. 2022. PAC-Bayes Information Bottleneck. In *ICLR*.
- [35] Junde Wu, Rao Fu, Huihui Fang, Yu Zhang, and Yanwu Xu. 2023. MedSegDiff-V2: Diffusion based Medical Image Segmentation with Transformer. *ArXiv abs/2301.11798 (2023)*.
- [36] Jiangbin Zheng, Yile Wang, Cheng Tan, Siyuan Li, Ge Wang, Jun Xia, Yidong Chen, and Stan Z. Li. 2023. CVT-SLR: Contrastive Visual-Textual Transformation for Sign Language Recognition with Variational Alignment. *ArXiv (2023)*. <https://doi.org/10.48550/arXiv.2303.05725>
- [37] Hao Zhou, Wengang Zhou, Weizhen Qi, Junfu Pu, and Houqiang Li. 2021. Improving Sign Language Translation with Monolingual Data by Sign Back-Translation. In *CVPR*.
- [38] Zixin Zhu, Yixuan Wei, Jianfeng Wang, Zhe Gan, Zheng Zhang, Le Wang, Gang Hua, Lijuan Wang, Zicheng Liu, and Han Hu. 2022. Exploring Discrete Diffusion Models for Image Captioning. *ArXiv (2022)*.
- [39] Ronglai Zuo and Brian Mak. 2022. C2SLR: Consistency-Enhanced Continuous Sign Language Recognition. In *CVPR*. 5131–5140.

A EFFECTS OF THE AUTOENCODER-FORMED CONDITIONAL DIFFUSION FEATURE REFINEMENT

In this section, we will further evaluate the effectiveness of the proposed autoencoder-formed conditional diffusion feature refinement (ACDR) by computing not only the word error rate (WER) metric but also the information stored in weights (IIW) [34] for distinct state-of-the-art methods. The experiment results are presented in Table 8. IIW is a metric designed to compute the amount of information in the feature representation, which can indicate the generalization gap between the network loss on the training and test datasets. Therefore, it is an appropriate metric for measuring the generalization ability of the sequence representations. As shown in Table 8, when all state-of-the-art methods are enhanced with ACDR, they achieve lower generalization gap (lower IIW) and enhanced performance (lower WER). It is worth noting that adding ACDR to refine the sequence representation consistently leads to lower IIW values, not only achieving a lower IIW of the sequence representation (see V-IIW), but also gaining a lower IIW of both the spatial representation and the gloss-wise temporal representation (see sp-IIW and gwt-IIW). These findings demonstrate that ACDR can effectively refine the sequence representation by providing informative gloss-wise dependencies and discriminative glosses context semantics via the diffusion process. Moreover, the refined sequence representations provide adequate short-long temporal dependencies to the classifier, resulting in robust feedback for both the visual module and spatial module, which implicitly enhances them and mitigates the sequence module overfitting problem.

Table 8: Compatibility (WER ↓ and IIW [34] ↓ metrics) to distinct state-of-the-art methods on the RWTH-2014 dataset. sp-IIW, gwt-IIW and V-IIW denote the IIW value computing by the spatial representation, the gloss-wise temporal representation, and the sequence representation.

Methods	sp-IIW	gwt-IIW	V-IIW	Dev (%)	Test (%)
VAC	1.9E-8	9.5E-7	2.5E-8	21.1	22.3
+ACDR	1.0E-8	2.1E-7	1.1E-8	20.5	20.6
SEN	1.3E-9	1.1E-7	7.8E-10	19.5	21.0
+ACDR	3.7E-10	9.4E-8	1.7E-10	18.8	20.0
TLP	1.8E-9	5.1E-8	2.4E-8	19.7	20.8
+ACDR	1.1E-9	2.1E-8	2.7E-10	19.0	20.0
CorrNet	6.3E-8	3.3E-7	6.9E-9	19.0	19.7
+ACDR	6.5E-9	8.5E-8	1.1E-9	18.6	19.0

B QUALITATIVE COMPLEMENTARY EXPERIMENTS

In this section, to assess the quality of ACDR, we employ visualizations of heatmaps for self-similarity matrices of gloss-wise temporal representation X_{gwt} and sequence representation V , as well as similarity matrices between V and X_{gwt} for qualitative evaluation. Experiments are given in Figure 6, Figure 7, Figure 8, Figure 9,

Figure 10, and Figure 11. The evaluated sample in both Figure 6 and Figure 7 is the video “01April-2010-Thursday-heute-default-5” in the RWTH-2014 [19] test set. The evaluated sample in both Figure 8 and Figure 9 is the video “15February-2011-Tuesday-heute-default-17” in the RWTH-2014 [19] test set. And the evaluated sample in both Figure 10 and Figure 11 is the video “31March-2010-Wednesday-tagesschau-default-11” in the RWTH-2014 [19] test set.

Figure 6 illustrates the impact of the ACDR and the ACDR only equips with the gloss-wise semantic condition P^{tc} on the sequence representations of the VAC model. Specifically, when the VAC replaces its knowledge distillation loss (VA loss) with the ACDR $^{P^{tc}}$ optimization, the self-similarity of the gloss-wise temporal representation X_{gwt} changed a little, while the self-similarity of the sequence representations V and the similarity between X_{gwt} and V increase significantly. Notably, the similarity matrix between X_{gwt} and V reveals that a few features in V are highly similar to all features of X_{gwt} . These experimental results demonstrate that the sequence representations optimized by ACDR have the capability to generate informative gloss-wise temporal dependencies. Furthermore, when comparing VAC+ACDR with VAC+ACDR $^{P^{tc}}$, we observe that introducing the gloss semantic condition leads to a remarkable similarity increase in the self-similarity matrix of X_{gwt} . This finding suggests that feeding the sequence representations into the discriminative semantics among glosses can enhance their generalization ability, resulting in more robust feedback for the visual module.

To comprehensively illustrate the properties of the ACDR, more similarity matrices heatmaps visualizations of distinct state-of-the-art methods with distinct samples are shown in Figure 7, Figure 8, Figure 9, Figure 10, and Figure 11. And we can observe that all of the results show a similar characteristic with the instance we gave in Figure 6. The CorrNet model’s sequence representations V have been observed to focus on the nearby gloss-wise temporal representation X_{gwt} , based on the SMKD [11]. After the ACDR optimization, the sequence representations exhibit an even stronger focus on the nearby gloss-wise temporal representation. Moreover, the impact of ACDR on different models, including VAC, SEN, TLP, and CorrNet, is evident from the similarity matrix heatmaps in Figure 6 and Figures 8-11. The ACDR optimization demonstrates a more significant improvement in the VAC, SEN, and TLP models, corresponding to their improved word error rate (WER) performance.

In summary, the above experimental results indicate that ACDR can effectively refine the sequence representations by incorporating informative gloss-wise dependencies and discriminative glosses context semantics via the diffusion process, which are essential for enhancing the generalization ability. Moreover, the refined sequence representations will result in more robust feedback for both the visual module and spatial module, which implicitly enhances them and mitigates the sequence module overfitting problem.

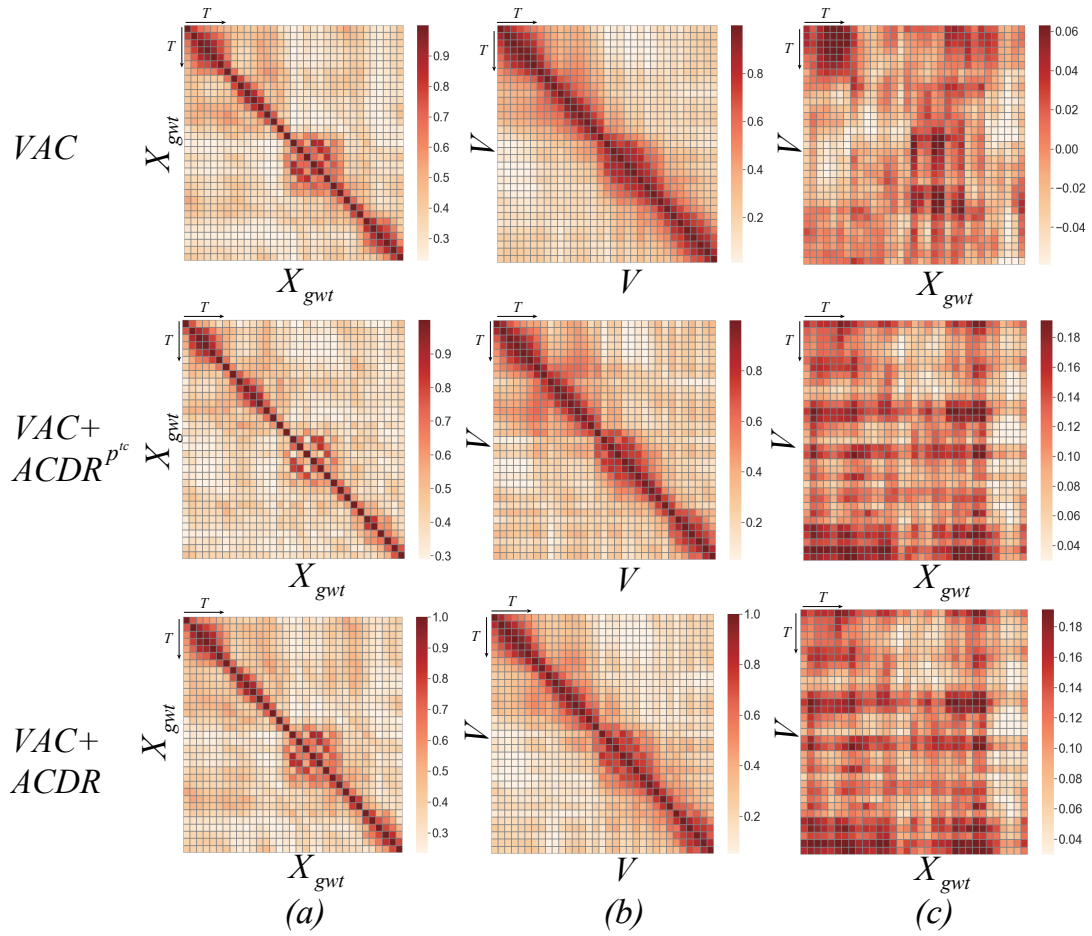


Figure 6: The visualizations of heatmaps for self-similarity matrices of gloss-wise temporal representation X_{gwt} and sequence representation V , as well as similarity matrices between V and X_{gwt} (the darker color represents the higher similarity). VAC+ACDR^{P^{tc}} refers to the VAC with its knowledge distillation loss (VA loss) replaced by ACDR optimization equipped with gloss-wise semantic condition P^{tc} . VAC+ACDR denotes the VAC enhanced by ACDR with both gloss-wise temporal semantic conditions and gloss semantic conditions.

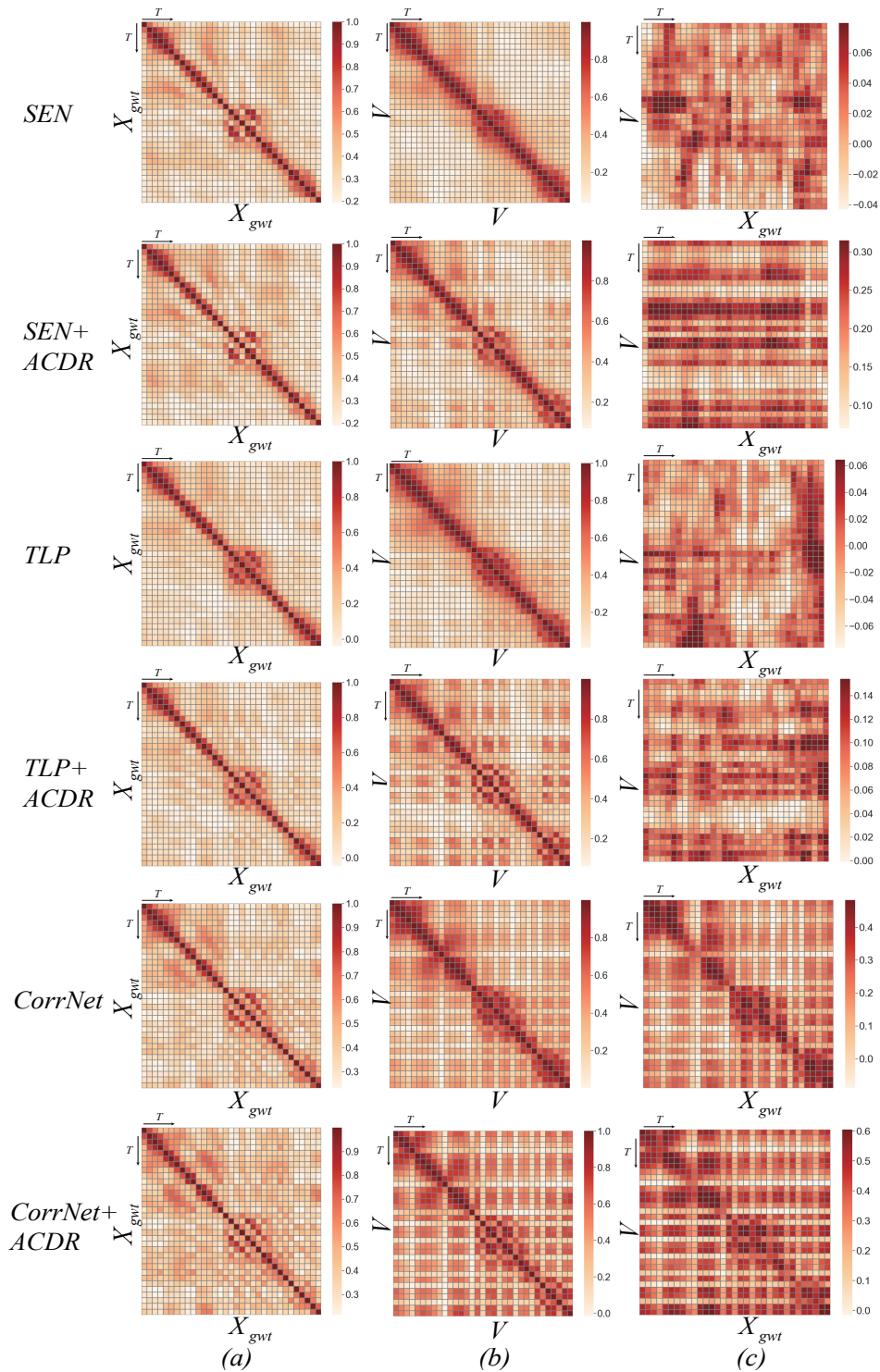


Figure 7: The visualization of similarity matrix heatmaps for the gloss-wise temporal representation X_{gwt} and the sequence representation V of the state-of-the-art methods. The heatmaps are organized into three columns: (a) and (b) columns depict the self-similarity matrix heatmaps of X_{gwt} and V , respectively, while the last column shows the similarity matrix heatmap between V and X_{gwt} (with darker colors indicating higher similarity).

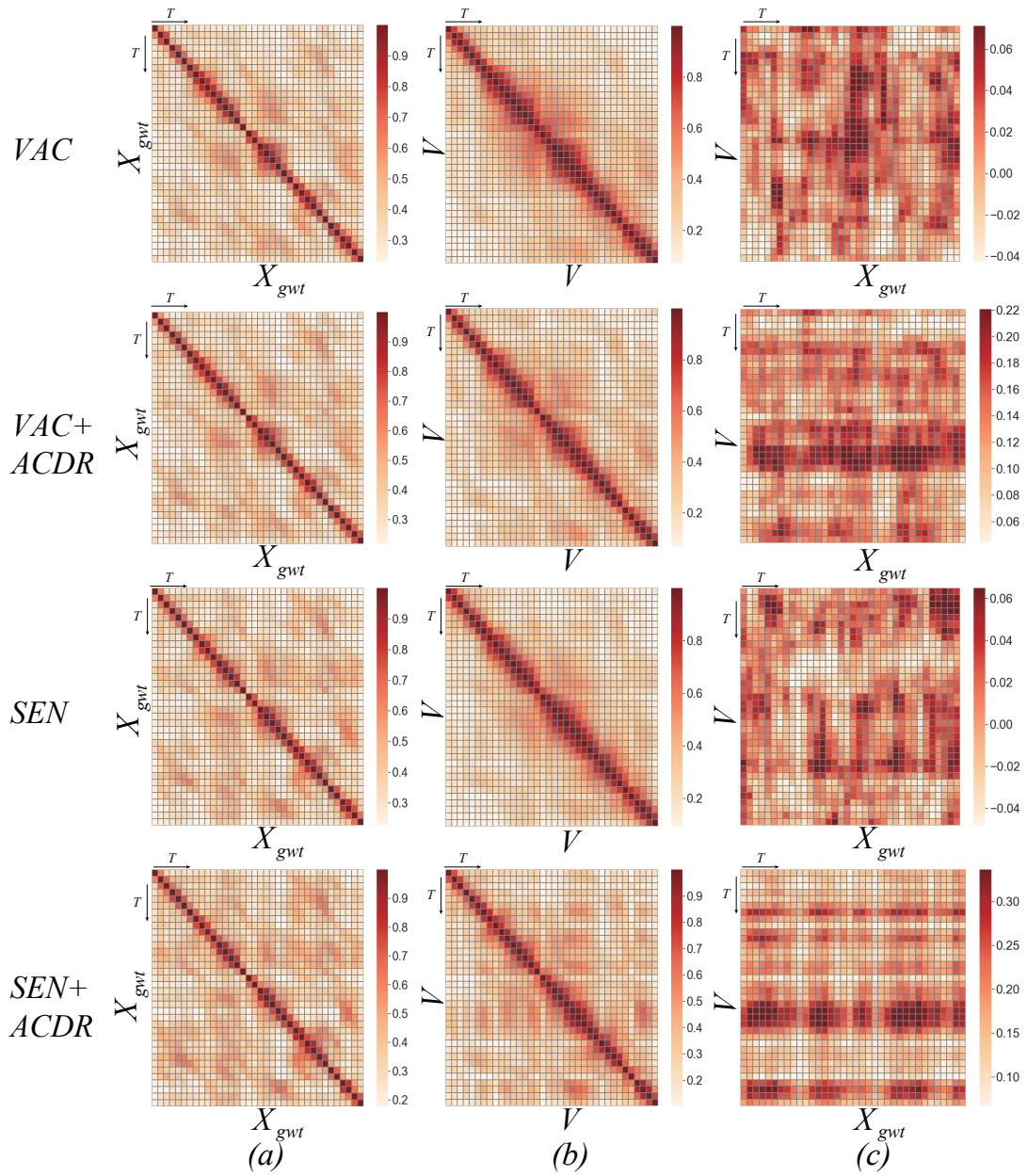


Figure 8: The visualization of similarity matrix heatmaps for the gloss-wise temporal representation X_{gwt} and the sequence representation V of the state-of-the-art methods. The heatmaps are organized into three columns: (a) and (b) columns depict the self-similarity matrix heatmaps of X_{gwt} and V , respectively, while the last column shows the similarity matrix heatmap between V and X_{gwt} (with darker colors indicating higher similarity).

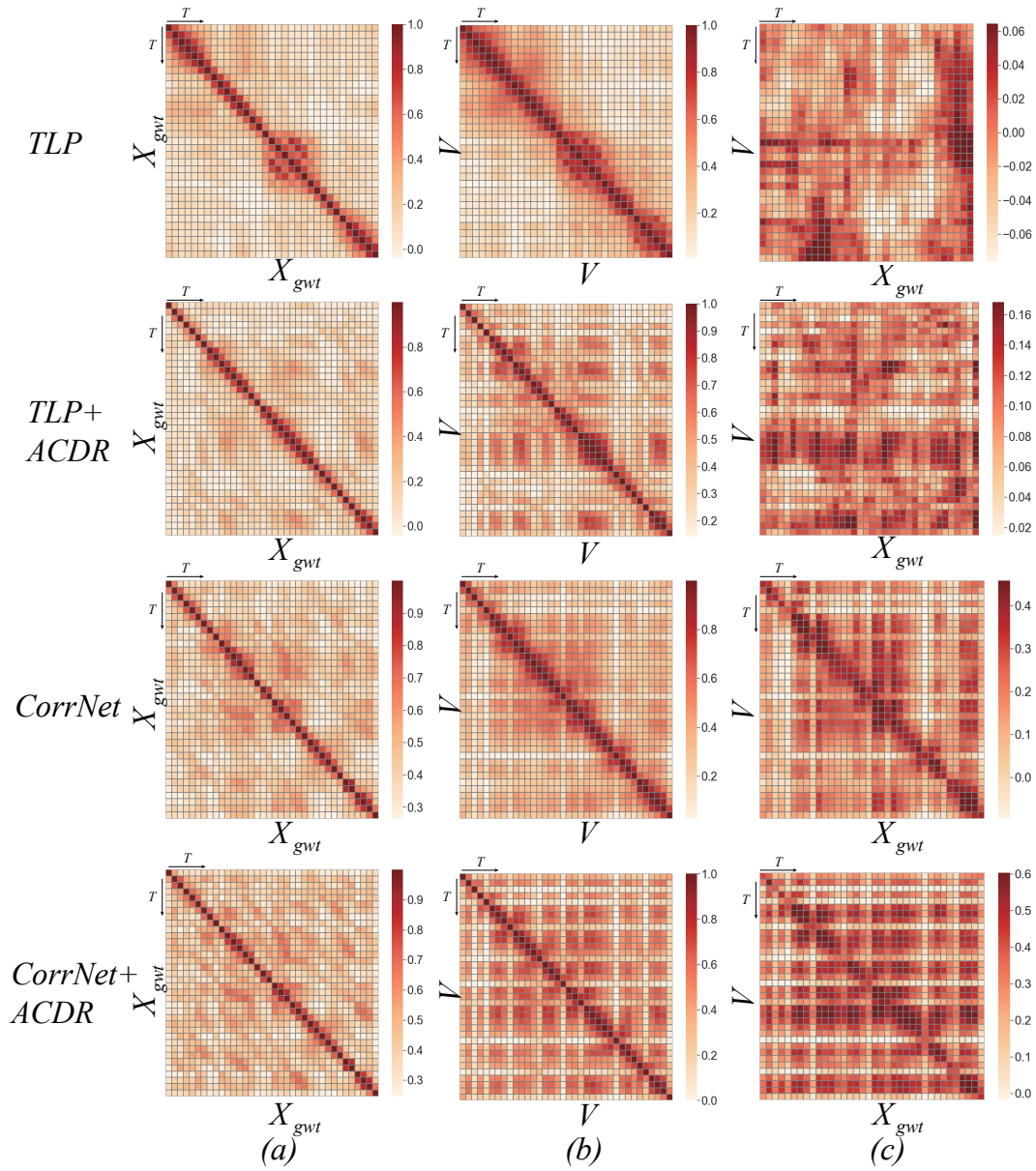


Figure 9: The visualization of similarity matrix heatmaps for the gloss-wise temporal representation X_{gwt} and the sequence representation V of the state-of-the-art methods. The heatmaps are organized into three columns: (a) and (b) columns depict the self-similarity matrix heatmaps of X_{gwt} and V , respectively, while the last column shows the similarity matrix heatmap between V and X_{gwt} (with darker colors indicating higher similarity).

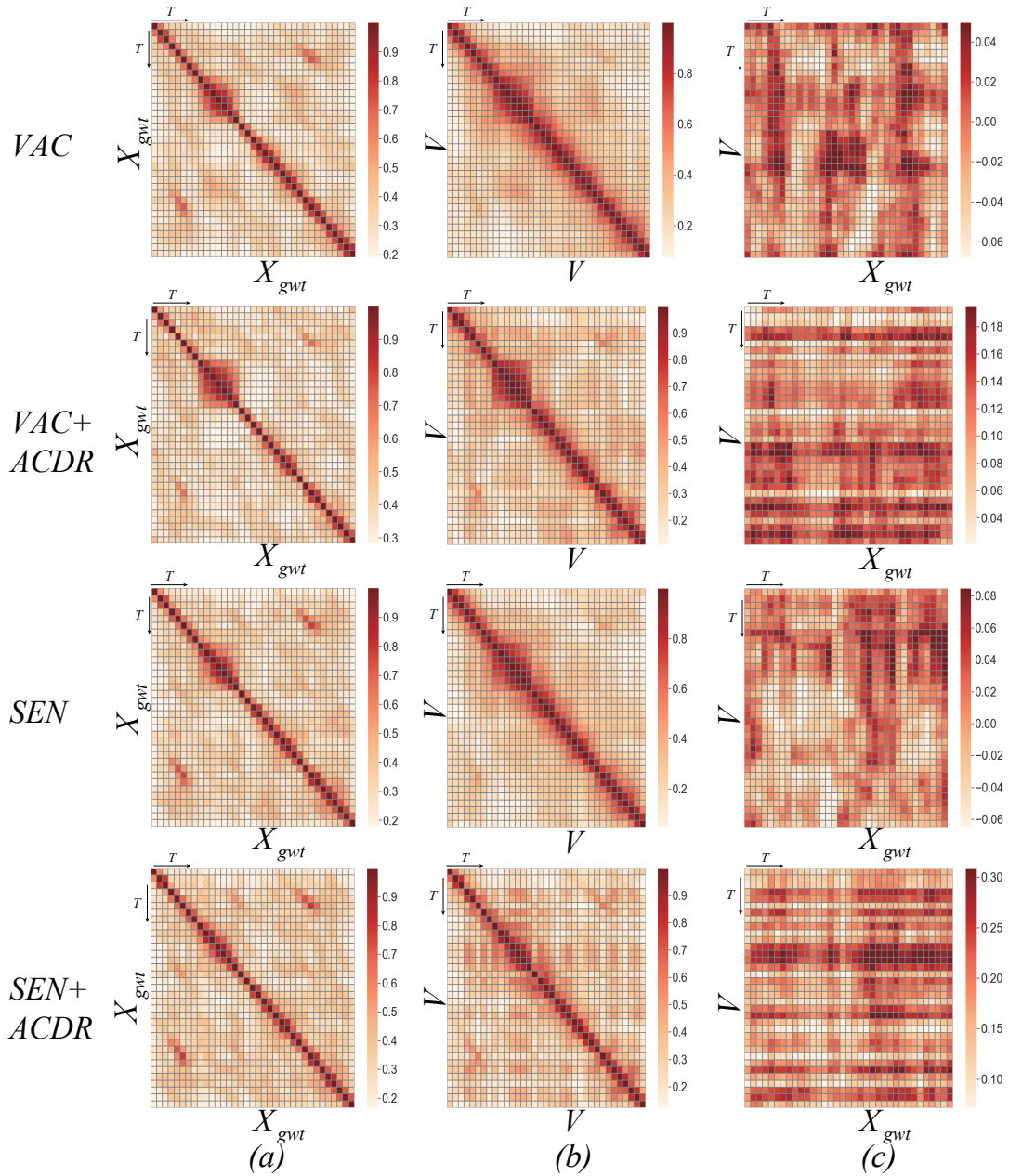


Figure 10: The visualization of similarity matrix heatmaps for the gloss-wise temporal representation X_{gwt} and the sequence representation V of the state-of-the-art methods. The heatmaps are organized into three columns: (a) and (b) columns depict the self-similarity matrix heatmaps of X_{gwt} and V , respectively, while the last column shows the similarity matrix heatmap between V and X_{gwt} (with darker colors indicating higher similarity).

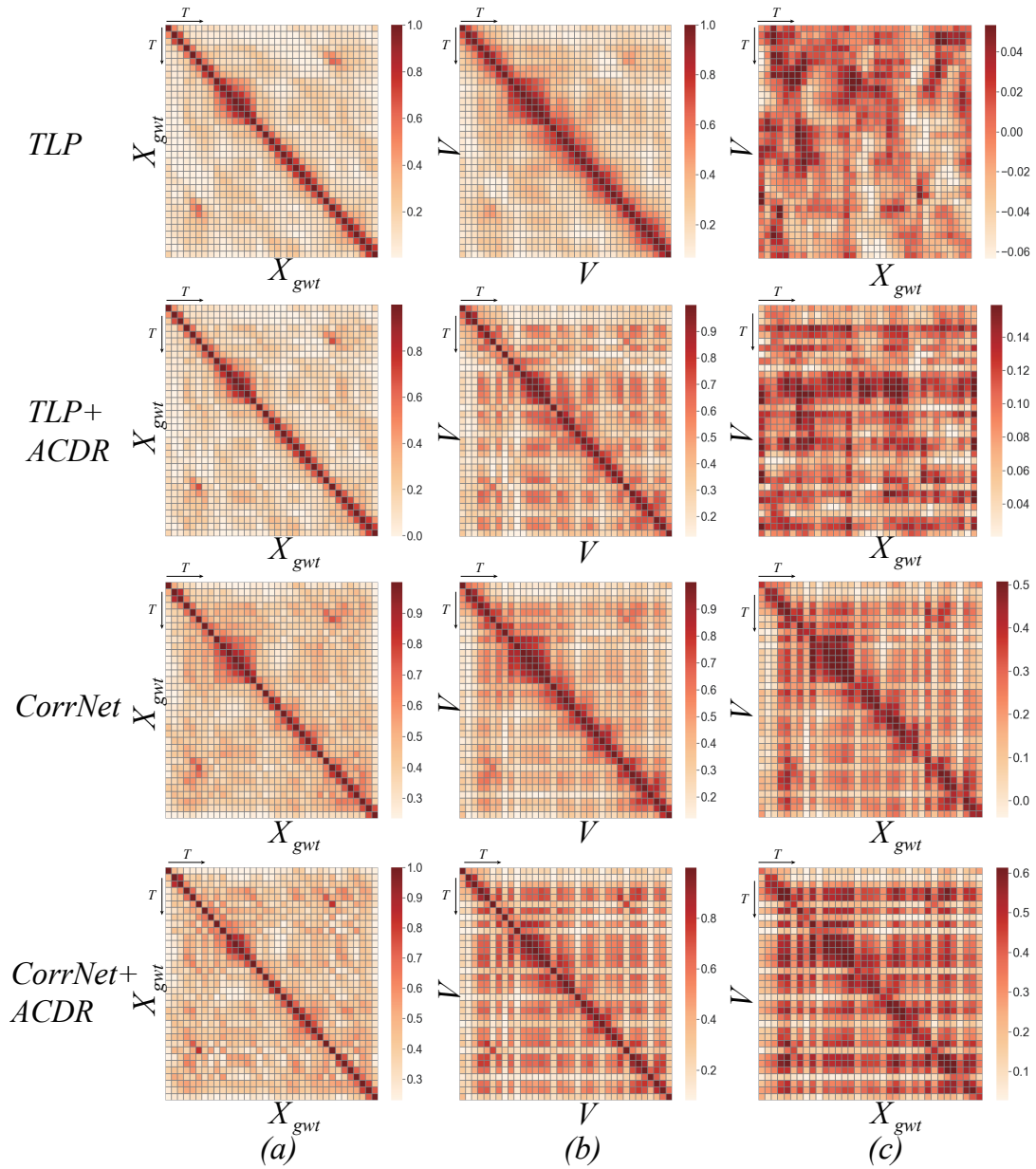


Figure 11: The visualization of similarity matrix heatmaps for the gloss-wise temporal representation X_{gwt} and the sequence representation V of the state-of-the-art methods. The heatmaps are organized into three columns: (a) and (b) columns depict the self-similarity matrix heatmaps of X_{gwt} and V , respectively, while the last column shows the similarity matrix heatmap between V and X_{gwt} (with darker colors indicating higher similarity).